

Article

# Casimir Interaction of Chern–Simons Layers on Substrates via Vacuum Stress Tensor

Valery N. Marachevsky \* and Arseny A. Sidelnikov 

Saint-Petersburg State University, 7/9 Universitetskaya nab., 199034 St. Petersburg, Russia;  
st074065@student.spbu.ru

\* Correspondence: maraval@mail.ru or v.marachevsky@spbu.ru

**Abstract:** We develop a Green’s functions scattering method for systems with Chern–Simons plane boundary layers on dielectric half-spaces. The Casimir pressure is derived by evaluation of the stress tensor in a vacuum slit between two half-spaces. The sign of the Casimir pressure on a Chern–Simons plane layer separated by a vacuum slit from the Chern–Simons layer at the boundary of a dielectric half-space is analyzed for intrinsic Si and SiO<sub>2</sub> glass substrates.

**Keywords:** Casimir pressure; stress tensor; Chern–Simons layer

## 1. Introduction

Quantum interaction between macroscopic bodies in the ground state is studied via the Casimir effect [1,2]—various reviews and books are dedicated to the subject [3–24]. The Lifshitz formula [25] determines the interaction between two dielectric half-spaces separated by a vacuum slit; it determines interaction due to fluctuations in the relevant case when transverse electric (TE) and transverse magnetic (TM) polarizations of the electromagnetic field do not mix after reflection from flat boundaries of dielectrics. In this case, the Casimir pressure is attractive for dielectric half-spaces separated by a vacuum slit [26].

Nevertheless, there exist systems with plane boundaries and Casimir repulsive pressure. The Casimir pressure is repulsive for three dielectric media with plane-parallel boundaries when the inequality for dielectric permittivities  $\epsilon_1(i\omega) < \epsilon_2(i\omega) < \epsilon_3(i\omega)$  holds [27] with  $\omega$  the frequency; here, the medium with a dielectric permittivity  $\epsilon_2(\omega)$  fills the space between dielectrics with permittivities  $\epsilon_1(\omega)$  and  $\epsilon_3(\omega)$ . The experiment [28] has demonstrated that the sign of the Casimir–Lifshitz force can indeed be changed from attractive to repulsive by a suitable selection of interacting materials immersed in a fluid. The contribution of surface modes in three-layered systems guaranteeing repulsion has been investigated in Ref. [29], where it was demonstrated that at short separations, surface modes play a decisive role in the Casimir repulsion. The repulsive critical Casimir forces emerging in a critical binary liquid mixture near the critical temperature can be used to counteract attraction due to fluctuating Casimir–Lifshitz forces [30].

Another possibility to obtain the Casimir repulsion is to study the interaction between plates with dielectric, diamagnetic and magnetodielectric properties [31–35]. The pressure between a perfectly conducting plate and an infinitely permeable plate is derived by Timothy Boyer [36]; the pressure is purely repulsive in this case: its magnitude is 7/8 that of the Casimir pressure between two perfectly conducting plates [2]. Casimir pressure and repulsion between metamaterials were investigated in Refs. [37–40].

One can also obtain Casimir repulsion in systems with plane-parallel Chern–Simons layers [41,42]. There is a mixing of TE and TM polarizations of the electromagnetic field after reflection from the Chern–Simons layer [42]. The general result for the Casimir energy of two arbitrary Chern–Simons layers in vacuum is expressed through nondiagonal reflection matrices on the basis of TE and TM polarizations [42]. This structure of reflection



**Citation:** Marachevsky, V.N.; Sidelnikov, A.A. Casimir Interaction of Chern–Simons Layers on Substrates via Vacuum Stress Tensor. *Physics* **2024**, *6*, 496–514. <https://doi.org/10.3390/physics6020033>

Received: 30 December 2023

Revised: 21 January 2024

Accepted: 4 February 2024

Published: 2 April 2024



**Copyright:** © 2024 by the authors. Licensee MDPI, Basel, Switzerland. This article is an open access article distributed under the terms and conditions of the Creative Commons Attribution (CC BY) license (<https://creativecommons.org/licenses/by/4.0/>).

matrices leads to the Casimir attraction or the Casimir repulsion in systems with plane-parallel Chern–Simons layers in vacuum and at the boundaries of dielectrics, depending on the parameters of the layers [41–44]. The Monte Carlo method was used to calculate the Casimir energy of interacting Chern–Simons layers in vacuum in Refs. [45,46].

Maxwell–Chern–Simons (2 + 1) space-time dimensional Abelian electrodynamics with the Chern–Simons term was considered in Ref. [47]; there is a massive spin-1 excitation in this case. The constant of the Chern–Simons action is dimensionless in the (3 + 1) case. The study of the Casimir energy in systems with Chern–Simons terms in (3 + 1) dimensions was started in Refs. [48,49] in the framework of rigid, nonpenetrable boundary conditions.

Physical systems are known to be described by the Chern–Simons action with a quantized constant of the action. In the low-energy effective theory of topological insulators, the term proportional to  $\theta \mathbf{E} \mathbf{H}$ , with  $\mathbf{E}$  and  $\mathbf{H}$  the electric and magnetic fields, respectively, is added to the standard electromagnetic energy density; integration of this term over the volume of the topological insulator yields boundary Chern–Simons action. Chern–Simons boundary action is defined in this case by a dimensionless quantized parameter  $a$ :  $a = \alpha\theta/(2\pi)$ ,  $\theta = (2n + 1)\pi$ , where  $\alpha$  is a fine structure constant of quantum electrodynamics and  $n$  is an integer number [50]. The Casimir effect for topological insulators was studied in Refs. [51–56].

In the non-dispersive case, Chern insulators [57–59] are described by the Chern–Simons action with a quantized parameter  $a = C\alpha$ , where  $C$  is a Chern number equal to the winding number of a map from a two-dimensional torus to a two-dimensional unit sphere. The Casimir effect for Chern insulators was investigated in Refs. [42,60,61].

For quantum Hall layers in an external magnetic field, the quantized parameter of the Chern–Simons action characterizing Hall plateaus takes the values  $a = \nu\alpha$ , where  $\nu$  is an integer or a fractional number [43,62,63].

Recently, the formalism based on Green’s functions scattering has been worked out [3,64]; in this approach, one evaluates the Casimir pressure in an explicit gauge-invariant derivation. The formalism yields gauge-invariant results for electric and magnetic Green’s functions by construction. Note that due to disregard of gauge invariance, the electric and the magnetic Green’s functions for the Lifshitz problem (two dielectric half-spaces separated by a vacuum slit) obtained in the book [4] contradict the result for the Casimir–Polder potential of a polarizable neutral atom located between two dielectric half-spaces [3,64].

The Casimir–Polder potential of a neutral anisotropic atom added to a multi-body system is expressed in the second-order perturbation theory in terms of electric Green’s functions for this system [3,65–68]. The Casimir–Polder potential of an anisotropic atom is repulsive at distances close to the hole in a plane conductor or grooves of a diffraction grating when the atomic polarizability is aligned in a direction perpendicular to the conductor [69,70] or a diffraction grating [71], in cylindrical and other geometries [72–76]. Note that the repulsion of the point charge from the axisymmetric conductor with an opening is present in electrostatics [77]. The curvature-induced repulsive effect on the lateral Casimir–Polder force is studied in Refs. [78–80]. The fundamental limits on the Casimir–Polder repulsive and attractive forces have been determined in Ref. [81].

The Casimir–Polder potential of a neutral anisotropic atom in the presence of a single Chern–Simons plane layer has been derived in Ref. [82]. The symmetric part of the polarizability for a nonmagnetic ground-state molecule yields potential proportional to the Casimir–Polder potential in front of a perfectly conducting plane; the asymmetric part of the polarizability also contributes to the Casimir–Polder potential [82]. Chiral media are actively studied in the Casimir effect [83,84]; the Casimir–Polder potential of a molecule with an isotropic chiral polarizability interacting with a chiral medium has been studied in Ref. [85]. Charge–parity violating effects [86] for the Casimir–Polder potential in the presence of a Chern–Simons layer have been studied in Ref. [87]; the Chern–Simons layer induces Casimir–Polder interaction both with a molecule that is not chiral but has an electric–magnetic cross polarizability and with a molecule having an anisotropic, asymmetric chiral polarizability. Recently, the formalism of Green’s functions scattering has been

applied to derive analytic results for the Casimir–Polder potentials of an anisotropic neutral atom in the presence of Chern–Simons plane boundary layers on dielectric half-spaces and in vacuum [88]. A novel three-body vacuum parity effect has been discovered in the system Chern–Simons layer–atom–Chern–Simons layer, which manifests as different values of the Casimir–Polder potential after a 180 degree rotation of one of the layers [88].

In this paper, we develop a Green’s functions scattering method and derive the Casimir pressure in geometries with Chern–Simons plane boundary layers on dielectric substrates by evaluation of the Casimir fluctuation pressure via vacuum stress tensor [3,4,25,64,89]. We proceed as follows. In Section 2, we derive expressions for the field of a point dipole in vacuum in terms of electric and magnetic fields. Then, we derive electric and magnetic Green’s functions in a slit between two dielectric substrate half-spaces covered by Chern–Simons layers. The Casimir pressure is expressed in terms of electric and magnetic Green’s functions through evaluation of the vacuum stress tensor in the slit. In Section 3, we study the sign of the Casimir pressure on a Chern–Simons plane layer separated by a vacuum slit from the Chern–Simons layer at the boundary of a dielectric half-space for intrinsic Si and SiO<sub>2</sub> glass substrates. Connection between representations of the Casimir energy in the local polar basis and the local basis of TE and TM polarizations in momentum space is established in Appendix A.

The magnetic permeability of materials  $\mu = 1$  throughout the text. We use  $\hbar = c = 1$  for the reduced Planck constant,  $\hbar$ , and the speed of light,  $c$ , and Heaviside–Lorentz units.

## 2. Casimir Pressure in the System of Two Dielectric Half-Spaces with Chern–Simons Boundary Layers

Consider the volume charge density ( $\rho$ ) and the current density ( $\mathbf{j}$ ) of a dipole source at the point  $\mathbf{r}' = (0, 0, z')$  [82]:

$$\rho(t, \mathbf{r}) = -p^l(t) \frac{\partial \delta^3(\mathbf{r} - \mathbf{r}')}{\partial x^l}, \tag{1}$$

$$j^l(t, \mathbf{r}) = \frac{\partial p^l(t)}{\partial t} \delta^3(\mathbf{r} - \mathbf{r}'), \tag{2}$$

where  $\mathbf{p}$  is an electric dipole moment vector,  $\mathbf{r} = (x, y, z)$ ,  $t$  denotes time, the Latin letter indices denote the space components and  $\delta^3(\cdot)$  is the three-dimensional Dirac delta function. The four-current density (1)–(2) satisfies the continuity equation  $\partial\rho/\partial t + \text{div}\mathbf{j} = 0$ .

The Weyl formula, [90]

$$\frac{e^{i\omega|\mathbf{r}'-\mathbf{r}|}}{4\pi|\mathbf{r}'-\mathbf{r}|} = i \iiint \frac{e^{i(k_x(x'-x)+k_y(y'-y)+\sqrt{\omega^2-k_x^2-k_y^2}(z'-z))}}{2\sqrt{\omega^2-k_x^2-k_y^2}} \frac{dk_x dk_y}{(2\pi)^2}, \tag{3}$$

valid for  $z' - z > 0$ , can be substituted into the solution of equations for scalar ( $\phi$ ) and vector ( $\mathbf{A}$ ) potentials:

$$(\Delta + \omega^2)\phi(\omega, \mathbf{r}) = -\rho(\omega, \mathbf{r}), \tag{4}$$

$$(\Delta + \omega^2)\mathbf{A}(\omega, \mathbf{r}) = -\mathbf{j}(\omega, \mathbf{r}) \tag{5}$$

to find electric and magnetic fields from a dipole source (1)–(2) in free space. As a result, electric and magnetic fields propagating upwards from the dipole source (1)–(2) in free space have the form [3]

$$\mathbf{E}_{\text{up}}^{(0)}(\omega, \mathbf{r}) = \int \mathbf{N}(\omega, \mathbf{k}_{\parallel}) e^{i\mathbf{k}_{\parallel} \cdot \mathbf{r}_{\parallel}} e^{ik_z(z-z')} d^2\mathbf{k}_{\parallel}, \tag{6}$$

$$\mathbf{H}_{\text{up}}^{(0)}(\omega, \mathbf{r}) = \frac{1}{\omega} \int [\mathbf{k} \times \mathbf{N}(\omega, \mathbf{k}_{\parallel})] e^{i\mathbf{k}_{\parallel} \cdot \mathbf{r}_{\parallel}} e^{ik_z(z-z')} d^2\mathbf{k}_{\parallel}, \tag{7}$$

$$\mathbf{N}(\omega, \mathbf{k}_{\parallel}) = \frac{i}{8\pi^2 k_z} \left( -(\mathbf{p} \cdot \mathbf{k})\mathbf{k} + \omega^2 \mathbf{p} \right), \tag{8}$$

where  $\mathbf{k}_{\parallel} = (k_x, k_y, 0)$ ,  $k_z = \sqrt{\omega^2 - k_{\parallel}^2}$ ,  $\mathbf{k} = (\mathbf{k}_{\parallel}, k_z)$  and  $\mathbf{r}_{\parallel} = (x, y, 0)$ .

We start from a solution of the diffraction problem of a dipole field when the dielectric medium is filling the half-space  $z > d$ . Scalar and vector functions defining the half-space  $z \geq d$  or diffraction from it are denoted by index 1. A homogeneous dielectric half-space  $z > d$  is characterized by a frequency dispersion of a dielectric permittivity  $\epsilon_1(\omega)$  at every point. In addition, there is a Chern–Simons plane layer at the boundary  $z = d$ . The Chern–Simons layer at  $z = d$  is described by the action

$$S_{\text{CS}} = \frac{a_1}{2} \int \epsilon^{z\nu\rho\sigma} A_{\nu} F_{\rho\sigma} dt dx dy \tag{9}$$

with a dimensionless parameter  $a_1$ ,  $\epsilon$  the Levi-Civita symbol,  $A_{\nu}$  the electromagnetic four-potential,  $F_{\rho\sigma} \equiv \partial_{\rho} A_{\sigma} - \partial_{\sigma} A_{\rho}$ , the Greek letter indices take Minkowski space-time values, and  $\partial_{\rho} \equiv \partial/\partial x^{\rho}$  over space-time coordinates.

Consider an upward propagation of the electromagnetic field from a point dipole (1)–(2). In the presence of a dielectric medium for  $z > d$ , one writes the solution of the Maxwell equations for  $z < d$  in the form

$$\mathbf{E}^{(V_1)}(\omega, \mathbf{r}) = \int \mathbf{N} e^{i\mathbf{k}_{\parallel} \cdot \mathbf{r}_{\parallel}} e^{ik_z(z-z')} d^2\mathbf{k}_{\parallel} + \int \mathbf{v}_1 e^{i\mathbf{k}_{\parallel} \cdot \mathbf{r}_{\parallel}} e^{-ik_z z} d^2\mathbf{k}_{\parallel}, \tag{10}$$

$$\begin{aligned} \mathbf{H}^{(V_1)}(\omega, \mathbf{r}) &= \frac{1}{\omega} \int [\mathbf{k} \times \mathbf{N}] e^{i\mathbf{k}_{\parallel} \cdot \mathbf{r}_{\parallel}} e^{ik_z(z-z')} d^2\mathbf{k}_{\parallel} \\ &+ \frac{1}{\omega} \int \left( [\mathbf{k}_{\parallel} \times \mathbf{v}_1] - k_z [\mathbf{n} \times \mathbf{v}_1] \right) e^{i\mathbf{k}_{\parallel} \cdot \mathbf{r}_{\parallel}} e^{-ik_z z} d^2\mathbf{k}_{\parallel}. \end{aligned} \tag{11}$$

The transmitted fields for  $z > d$  are written in the form

$$\mathbf{E}^{(D_1)}(\omega, \mathbf{r}) = \int \mathbf{u}_1 e^{i\mathbf{k}_{\parallel} \cdot \mathbf{r}_{\parallel}} e^{iK_{z1}z} d^2\mathbf{k}_{\parallel}, \tag{12}$$

$$\mathbf{H}^{(D_1)}(\omega, \mathbf{r}) = \frac{1}{\omega} \int \left( [\mathbf{k}_{\parallel} \times \mathbf{u}_1] + K_{z1} [\mathbf{n} \times \mathbf{u}_1] \right) e^{i\mathbf{k}_{\parallel} \cdot \mathbf{r}_{\parallel}} e^{iK_{z1}z} d^2\mathbf{k}_{\parallel}, \tag{13}$$

where  $K_{z1} = \sqrt{\epsilon_1(\omega)\omega^2 - k_x^2 - k_y^2}$  and  $\mathbf{n} = (0, 0, 1)$ . Vector functions  $\mathbf{v}_1(\omega, \mathbf{k}_{\parallel})$  and  $\mathbf{u}_1(\omega, \mathbf{k}_{\parallel})$  are found from the transversality of the reflected and transmitted fields and the boundary conditions imposed on the fields:

$$\text{div}(\mathbf{E}^{(V_1)} - \mathbf{E}_{\text{up}}^{(0)}) = 0, \tag{14}$$

$$\text{div} \mathbf{E}^{(D_1)} = 0, \tag{15}$$

$$E_x^{(V_1)}|_{z=d} = E_x^{(D_1)}|_{z=d}, \tag{16}$$

$$E_y^{(V_1)}|_{z=d} = E_y^{(D_1)}|_{z=d}, \tag{17}$$

$$H_x^{(D_1)}|_{z=d+} - H_x^{(V_1)}|_{z=d-} = 2a_1 E_x^{(V_1)}|_{z=d}, \tag{18}$$

$$H_y^{(D_1)}|_{z=d+} - H_y^{(V_1)}|_{z=d-} = 2a_1 E_y^{(V_1)}|_{z=d}. \tag{19}$$

Boundary conditions (18)–(19) have been used to describe the diffraction of a plane electromagnetic wave in a medium with a piecewise constant axion field [91] and in a medium with Chern–Simons layers [92].

Boundary conditions (14)–(19) can be imposed in cylindrical coordinates in a local orthogonal basis  $\mathbf{e}_r, \mathbf{e}_\varphi, \mathbf{e}_z$  in momentum space so that  $\mathbf{k}_\parallel = k_r \mathbf{e}_r, k_r = |\mathbf{k}_\parallel|$ :

$$u_{1r}k_r + K_{z1}u_{1z} = 0, \tag{20}$$

$$v_{1r}k_r - k_z v_{1z} = 0, \tag{21}$$

$$u_{1r}e^{iK_{z1}d} = v_{1r}e^{-ik_z d} + N_r e^{ik_z(d-z')}, \tag{22}$$

$$u_{1\varphi}e^{iK_{z1}d} = v_{1\varphi}e^{-ik_z d} + N_\varphi e^{ik_z(d-z')}, \tag{23}$$

$$k_z v_{1\varphi}e^{-ik_z d} - k_z N_\varphi e^{ik_z(d-z')} + K_{z1}u_{1\varphi}e^{iK_{z1}d} = -2a_1 u_{1r}e^{iK_{z1}d}, \tag{24}$$

$$-k_z v_{1r}e^{-ik_z d} - k_r v_{1z}e^{-ik_z d} + k_z N_r e^{ik_z(d-z')} - k_r N_z e^{ik_z(d-z')} - (K_{z1}u_{1r}e^{iK_{z1}d} - k_r u_{1z}e^{iK_{z1}d}) = -2a_1 u_{1\varphi}e^{iK_{z1}d}. \tag{25}$$

The solution of the transversality conditions (20)–(21) and boundary conditions (22)–(25) imposed at  $z = d$  yields

$$v_{1r} = \left[ -\frac{r_{TM_1} + a_1^2 T_1}{1 + a_1^2 T_1} N_r + \frac{k_z}{\omega} \frac{a_1 T_1}{1 + a_1^2 T_1} N_\varphi \right] e^{ik_z(2d-z')}, \tag{26}$$

$$v_{1\varphi} = \left[ -\frac{\omega}{k_z} \frac{a_1 T_1}{1 + a_1^2 T_1} N_r + \frac{r_{TE_1} - a_1^2 T_1}{1 + a_1^2 T_1} N_\varphi \right] e^{ik_z(2d-z')}, \tag{27}$$

$$v_{1z} = -\frac{k_r}{k_z} \left[ \frac{r_{TM_1} + a_1^2 T_1}{1 + a_1^2 T_1} N_r - \frac{k_z}{\omega} \frac{a_1 T_1}{1 + a_1^2 T_1} N_\varphi \right] e^{ik_z(2d-z')}, \tag{28}$$

where the Fresnel reflection coefficients

$$r_{TM_1} = \frac{\varepsilon_1(\omega)k_z - K_{z1}}{\varepsilon_1(\omega)k_z + K_{z1}}, \quad r_{TE_1} = \frac{k_z - K_{z1}}{k_z + K_{z1}} \tag{29}$$

and

$$T_1 = \frac{4k_z K_{z1}}{(k_z + K_{z1})(\varepsilon_1(\omega)k_z + K_{z1})}. \tag{30}$$

depend on the dielectric permittivity  $\varepsilon_1(\omega)$  of the half-space  $z > d$ .

Electric and magnetic fields propagating downwards from the dipole source (1)–(2) in free space have the form [3]

$$\mathbf{E}_{\text{down}}^{(0)}(\omega, \mathbf{r}) = \int \tilde{\mathbf{N}}(\omega, \mathbf{k}_\parallel) e^{i\mathbf{k}_\parallel \cdot \mathbf{r}_\parallel} e^{-ik_z(z-z')} d^2 \mathbf{k}_\parallel, \tag{31}$$

$$\mathbf{H}_{\text{down}}^{(0)}(\omega, \mathbf{r}) = \frac{1}{\omega} \int [\tilde{\mathbf{k}} \times \tilde{\mathbf{N}}(\omega, \mathbf{k}_\parallel)] e^{i\mathbf{k}_\parallel \cdot \mathbf{r}_\parallel} e^{-ik_z(z-z')} d^2 \mathbf{k}_\parallel, \tag{32}$$

$$\tilde{\mathbf{N}}(\omega, \mathbf{k}_\parallel) = \frac{i}{8\pi^2 k_z} \left( -(\mathbf{p} \cdot \tilde{\mathbf{k}}) \tilde{\mathbf{k}} + \omega^2 \mathbf{p} \right), \tag{33}$$

where  $\tilde{\mathbf{k}} = (\mathbf{k}_\parallel, -k_z)$ .

The next step is to find a solution of the diffraction problem of a dipole field when the medium is filling half-space  $z < 0$ . Scalar and vector functions defining the half-space  $z \leq 0$  or diffraction from it are denoted by index 2. A homogeneous dielectric half-space  $z < 0$  is characterized by a frequency dispersion of a dielectric permittivity  $\varepsilon_2(\omega)$  at every point. There is a Chern–Simons plane layer characterized by a dimensionless parameter  $a_2$  at the boundary  $z = 0$ .

In the presence of a dielectric medium for  $z < 0$ , one adds the reflected parts of fields to a solution (31)–(32) and writes the solution of the Maxwell equations for  $z > 0$  in the form

$$\mathbf{E}^{(V_2)}(\omega, \mathbf{r}) = \int \tilde{\mathbf{N}}(\omega, \mathbf{k}_{\parallel}) e^{i\mathbf{k}_{\parallel} \cdot \mathbf{r}_{\parallel}} e^{-ik_z(z-z')} d^2\mathbf{k}_{\parallel} + \int \mathbf{v}_2(\omega, \mathbf{k}_{\parallel}) e^{i\mathbf{k}_{\parallel} \cdot \mathbf{r}_{\parallel}} e^{ik_z z} d^2\mathbf{k}_{\parallel}, \quad (34)$$

$$\begin{aligned} \mathbf{H}^{(V_2)}(\omega, \mathbf{r}) &= \frac{1}{\omega} \int [\tilde{\mathbf{k}} \times \tilde{\mathbf{N}}(\omega, \mathbf{k}_{\parallel})] e^{i\mathbf{k}_{\parallel} \cdot \mathbf{r}_{\parallel}} e^{-ik_z(z-z')} d^2\mathbf{k}_{\parallel} \\ &+ \frac{1}{\omega} \int [\mathbf{k} \times \mathbf{v}_2(\omega, \mathbf{k}_{\parallel})] e^{i\mathbf{k}_{\parallel} \cdot \mathbf{r}_{\parallel}} e^{ik_z z} d^2\mathbf{k}_{\parallel}. \end{aligned} \quad (35)$$

For  $z < 0$ , one writes the transmitted fields in the form

$$\mathbf{E}^{(D_2)}(\omega, \mathbf{r}) = \int \mathbf{u}_2(\omega, \mathbf{k}_{\parallel}) e^{i\mathbf{k}_{\parallel} \cdot \mathbf{r}_{\parallel}} e^{-iK_{z2}z} d^2\mathbf{k}_{\parallel}, \quad (36)$$

$$\mathbf{H}^{(D_2)}(\omega, \mathbf{r}) = \frac{1}{\omega} \int \left( [\mathbf{k}_{\parallel} \times \mathbf{u}_2(\omega, \mathbf{k}_{\parallel})] - K_{z2}[\mathbf{n} \times \mathbf{u}_2(\omega, \mathbf{k}_{\parallel})] \right) e^{i\mathbf{k}_{\parallel} \cdot \mathbf{r}_{\parallel}} e^{-iK_{z2}z} d^2\mathbf{k}_{\parallel}, \quad (37)$$

where  $K_{z2} = \sqrt{\epsilon_2(\omega)\omega^2 - k_x^2 - k_y^2}$  and  $\mathbf{n} = (0, 0, 1)$ . Vector functions  $\mathbf{v}_2(\omega, \mathbf{k}_{\parallel})$  and  $\mathbf{u}_2(\omega, \mathbf{k}_{\parallel})$  are found from the transversality of the reflected and transmitted fields and the boundary conditions imposed on the fields:

$$\text{div}(\mathbf{E}^{(V_2)} - \mathbf{E}_{\text{down}}^{(0)}) = 0, \quad (38)$$

$$\text{div} \mathbf{E}^{(D_2)} = 0, \quad (39)$$

$$E_x^{(V_2)}|_{z=0} = E_x^{(D_2)}|_{z=0}, \quad (40)$$

$$E_y^{(V_2)}|_{z=0} = E_y^{(D_2)}|_{z=0}, \quad (41)$$

$$H_x^{(V_2)}|_{z=0+} - H_x^{(D_2)}|_{z=0-} = 2a_2 E_x^{(V_2)}|_{z=0}, \quad (42)$$

$$H_y^{(V_2)}|_{z=0+} - H_y^{(D_2)}|_{z=0-} = 2a_2 E_y^{(V_2)}|_{z=0}. \quad (43)$$

It is convenient to write boundary conditions (38)–(43) in cylindrical coordinates in a local orthogonal basis  $\mathbf{e}_r, \mathbf{e}_\varphi, \mathbf{e}_z$  in momentum space so that  $\mathbf{k}_{\parallel} = k_r \mathbf{e}_r, k_r = |\mathbf{k}_{\parallel}|$ :

$$v_{2r} k_r + k_z v_{2z} = 0, \quad (44)$$

$$u_{2r} k_r - K_{z2} u_{2z} = 0, \quad (45)$$

$$u_{2r} = v_{2r} + \tilde{N}_r e^{ik_z z'}, \quad (46)$$

$$u_{2\varphi} = v_{2\varphi} + \tilde{N}_\varphi e^{ik_z z'}, \quad (47)$$

$$-k_z v_{2\varphi} + k_z \tilde{N}_\varphi e^{ik_z z'} - K_{z2} u_{2\varphi} = 2\omega a_2 u_{2r}, \quad (48)$$

$$k_z v_{2r} - k_r v_{2z} - k_z \tilde{N}_r e^{ik_z z'} - k_r \tilde{N}_z e^{ik_z z'} + K_{z2} u_{2r} + k_r u_{2z} = 2\omega a_2 u_\varphi \quad (49)$$

and get

$$v_{2r} = \left[ -\frac{r_{\text{TM}2} + a_2^2 T_2}{1 + a_2^2 T_2} \tilde{N}_r + \frac{k_z}{\omega} \frac{a_2 T_2}{1 + a_2^2 T_2} \tilde{N}_\varphi \right] e^{ik_z z'}, \quad (50)$$

$$v_{2\varphi} = \left[ -\frac{\omega}{k_z} \frac{a_2 T_2}{1 + a_2^2 T_2} \tilde{N}_r + \frac{r_{\text{TE}2} - a_2^2 T_2}{1 + a_2^2 T_2} \tilde{N}_\varphi \right] e^{ik_z z'}, \quad (51)$$

$$v_{2z} = \frac{k_r}{k_z} \left[ \frac{r_{\text{TM}2} + a_2^2 T_2}{1 + a_2^2 T_2} \tilde{N}_r - \frac{k_z}{\omega} \frac{a_2 T_2}{1 + a_2^2 T_2} \tilde{N}_\varphi \right] e^{ik_z z'}, \quad (52)$$

where Fresnel reflection coefficients  $r_{TM_2}$ ,  $r_{TE_2}$  and  $T_2$  depend on the dielectric permittivity  $\epsilon_2(\omega)$  of the half-space  $z < 0$ . The local matrix  $R$  resulting from Equations (26), (27), (50) and (51) is defined as follows:

$$R(a, \epsilon(\omega), \omega, k_r) \equiv \frac{1}{1 + a^2 T} \begin{pmatrix} -r_{TM} - a^2 T & \frac{k_z}{\omega} a T \\ -\frac{\omega}{k_z} a T & r_{TE} - a^2 T \end{pmatrix}. \tag{53}$$

The solution of a diffraction problem when both half-spaces are present simultaneously and the point dipole is located at  $\mathbf{r}' = (0, 0, z')$ ,  $0 < z' < d$  can be derived as follows. Denote the upper dielectric half-space ( $z > d$ ) by index 1 and the lower dielectric half-space ( $z < 0$ ) by index 2. The Chern–Simons boundary layers at  $z = d$  and  $z = 0$  are defined by the parameters  $a_1$  and  $a_2$  as before (Figure 1). From (53) and the solutions for the diffraction cases considered above, we define local matrices  $R_1$  and  $R_2$  for reflection of the tangential components of the electric field from media above and below the point dipole, respectively:

$$R_1(\omega) \equiv R(a_1, \epsilon_1(\omega), \omega, k_r), \quad R_2(\omega) \equiv R(a_2, \epsilon_2(\omega), \omega, k_r). \tag{54}$$

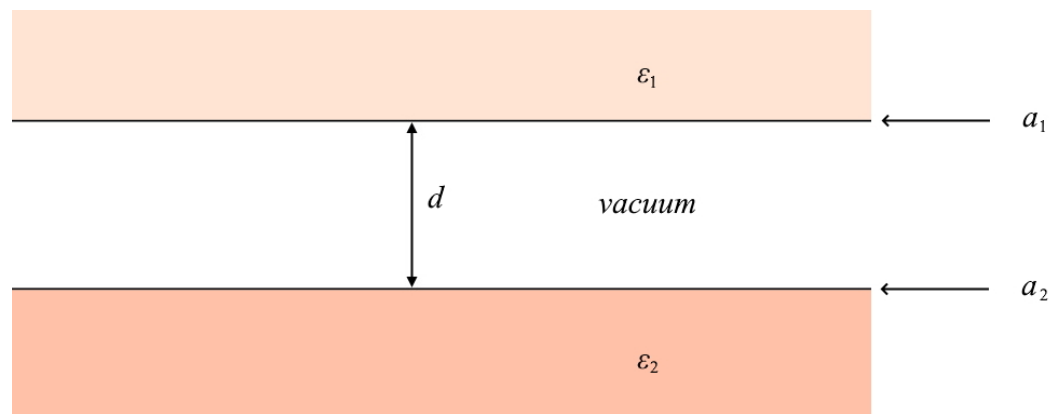


**Figure 1.** Two dielectric half-spaces with Chern–Simons boundary layers are separated by a distance  $d$ . The permittivity of the upper dielectric half-space is  $\epsilon_1$ ; the permittivity of the lower dielectric half-space is  $\epsilon_2$ . The upper Chern–Simons boundary layer is defined by  $a_1$ ; the lower Chern–Simons boundary layer is defined by  $a_2$ .

Tangential local components of the electric field in the interval  $0 < z < d$  from the point dipole (1)–(2) are expressed in terms of  $R_1, R_2$  after the summation of multiple reflections from media with indices 1 and 2:

$$\begin{pmatrix} E_r \\ E_\varphi \end{pmatrix} = \frac{I}{I - R_2 R_1 e^{2ik_z d}} e^{ik_z z} \left[ R_2 R_1 \begin{pmatrix} N_r \\ N_\varphi \end{pmatrix} e^{ik_z (2d - z')} + R_2 \begin{pmatrix} \widetilde{N}_r \\ \widetilde{N}_\varphi \end{pmatrix} e^{ik_z z'} \right] + \frac{I}{I - R_1 R_2 e^{2ik_z d}} e^{2ik_z d} e^{-ik_z z} \left[ R_1 R_2 \begin{pmatrix} \widetilde{N}_r \\ \widetilde{N}_\varphi \end{pmatrix} e^{ik_z z'} + R_1 \begin{pmatrix} N_r \\ N_\varphi \end{pmatrix} e^{-ik_z z'} \right], \tag{55}$$

where  $I$  is the identity matrix. From Equation (55), we define four matrices:

$$M^{(1)} \equiv (I - R_2(\omega) R_1(\omega) e^{i2k_z d})^{-1} R_2(\omega) R_1(\omega), \tag{56}$$

$$M^{(2)} \equiv (I - R_2(\omega) R_1(\omega) e^{i2k_z d})^{-1} R_2(\omega), \tag{57}$$

$$M^{(3)} \equiv (I - R_1(\omega) R_2(\omega) e^{i2k_z d})^{-1} R_1(\omega) R_2(\omega), \tag{58}$$

$$M^{(4)} \equiv (I - R_1(\omega) R_2(\omega) e^{i2k_z d})^{-1} R_1(\omega) \tag{59}$$

and write components of the electric field in a cylindrical local system of coordinates explicitly from Formulas (21), (44), (55) and (56)–(59):

$$E_r = e^{ik_z z} \left[ e^{-ik_z z'} e^{2ik_z d} (M_{11}^{(1)} N_r + M_{12}^{(1)} N_\varphi) + e^{ik_z z'} (M_{11}^{(2)} \widetilde{N}_r + M_{12}^{(2)} \widetilde{N}_\varphi) \right] + e^{-ik_z z} e^{2ik_z d} \left[ e^{ik_z z'} (M_{11}^{(3)} \widetilde{N}_r + M_{12}^{(3)} \widetilde{N}_\varphi) + e^{-ik_z z'} (M_{11}^{(4)} N_r + M_{12}^{(4)} N_\varphi) \right], \quad (60)$$

$$E_\varphi = e^{ik_z z} \left[ e^{-ik_z z'} e^{2ik_z d} (M_{21}^{(1)} N_r + M_{22}^{(1)} N_\varphi) + e^{ik_z z'} (M_{21}^{(2)} \widetilde{N}_r + M_{22}^{(2)} \widetilde{N}_\varphi) \right] + e^{-ik_z z} e^{2ik_z d} \left[ e^{ik_z z'} (M_{21}^{(3)} \widetilde{N}_r + M_{22}^{(3)} \widetilde{N}_\varphi) + e^{-ik_z z'} (M_{21}^{(4)} N_r + M_{22}^{(4)} N_\varphi) \right], \quad (61)$$

$$E_z = -\frac{k_r}{k_z} e^{ik_z z} \left[ e^{-ik_z z'} e^{2ik_z d} (M_{11}^{(1)} N_r + M_{12}^{(1)} N_\varphi) + e^{ik_z z'} (M_{11}^{(2)} \widetilde{N}_r + M_{12}^{(2)} \widetilde{N}_\varphi) \right] - e^{-ik_z z} e^{2ik_z d} \left[ e^{ik_z z'} (M_{11}^{(3)} \widetilde{N}_r + M_{12}^{(3)} \widetilde{N}_\varphi) + e^{-ik_z z'} (M_{11}^{(4)} N_r + M_{12}^{(4)} N_\varphi) \right], \quad (62)$$

where  $M_{11}^{(s)}, M_{12}^{(s)}, M_{21}^{(s)}, M_{22}^{(s)}$  ( $s = 1, \dots, 4$ ) are components of the four matrices (56)–(59).

For convenience, we rewrite  $\mathbf{N}$  and  $\widetilde{\mathbf{N}}$  in a cylindrical system of coordinates:

$$\mathbf{N} = \frac{i}{8\pi^2 k_z} \left( -(p_r k_r + k_z p_z)(\mathbf{e}_r k_r + \mathbf{e}_z k_z) + \omega^2 \mathbf{p} \right), \quad (63)$$

$$\widetilde{\mathbf{N}} = \frac{i}{8\pi^2 k_z} \left( -(p_r k_r - k_z p_z)(\mathbf{e}_r k_r - \mathbf{e}_z k_z) + \omega^2 \mathbf{p} \right). \quad (64)$$

The scattered part of the electric field at the point  $\mathbf{r}$  from the source (1)–(2) at the point  $\mathbf{r}'$  for  $0 < z, z' < d$  is given by

$$\mathbf{E}(\mathbf{r}, \mathbf{r}') = \int d^2 \mathbf{k}_\parallel e^{i\mathbf{k}_\parallel \cdot (\mathbf{r}_\parallel - \mathbf{r}'_\parallel)} (E_r \mathbf{e}_r + E_\varphi \mathbf{e}_\varphi + E_z \mathbf{e}_z). \quad (65)$$

The rotation formulas between a cylindrical local basis and a Cartesian basis for every given  $\mathbf{k}_\parallel$  are standard:

$$E_x = E_r \cos \varphi + E_\varphi \sin \varphi, \quad (66)$$

$$E_y = E_r \sin \varphi - E_\varphi \cos \varphi, \quad (67)$$

$$p_r = p_x \cos \varphi + p_y \sin \varphi, \quad (68)$$

$$p_\varphi = p_x \sin \varphi - p_y \cos \varphi, \quad (69)$$

where  $p_x$  and  $p_y$  denote the Cartesian components of an electric dipole moment vector.

The Cartesian components of the scattered electric Green's functions are expressed in terms of components of the reflected electric Green's functions in a cylindrical local basis from (66)–(69) for  $\mathbf{r}_\parallel = \mathbf{r}'_\parallel$ :

$$D_{xx}^E(\omega, z, z') = \int (D_{rr}^E(\omega, k_r, z, z') \cos^2 \varphi + D_{\varphi\varphi}^E(\omega, k_r, z, z') \sin^2 \varphi) \frac{d^2 \mathbf{k}_{\parallel}}{(2\pi)^2}, \quad (70)$$

$$D_{yy}^E(\omega, z, z') = \int (D_{rr}^E(\omega, k_r, z, z') \sin^2 \varphi + D_{\varphi\varphi}^E(\omega, k_r, z, z') \cos^2 \varphi) \frac{d^2 \mathbf{k}_{\parallel}}{(2\pi)^2}, \quad (71)$$

$$D_{zz}^E(\omega, z, z') = \int D_{zz}^E(\omega, k_r, z, z') \frac{d^2 \mathbf{k}_{\parallel}}{(2\pi)^2}, \quad (72)$$

In Equations (70)–(72), we omit nondiagonal contributions to scattered Green’s functions in a cylindrical local basis proportional to either  $\cos \varphi \sin \varphi$ ,  $\cos \varphi$  or  $\sin \varphi$  since integrals over angle  $\varphi$  equal zero for these terms for coinciding arguments  $\mathbf{r}_{\parallel} = \mathbf{r}'_{\parallel}$ .

The components of the scattered electric Green’s functions in a cylindrical local basis entering (70)–(72) are found from (60)–(64):

$$D_{rr}^E(\omega, k_r, z, z') = \frac{ik_z}{2} \times \left[ e^{ik_z(z-z')} e^{2ik_z d} M_{11}^{(1)} + e^{ik_z(z+z')} M_{11}^{(2)} + e^{ik_z(z'-z)} e^{2ik_z d} M_{11}^{(3)} + e^{-ik_z(z+z')} e^{2ik_z d} M_{11}^{(4)} \right], \quad (73)$$

$$D_{\varphi\varphi}^E(\omega, k_r, z, z') = \frac{i\omega^2}{2k_z} \times \left[ e^{ik_z(z-z')} e^{2ik_z d} M_{22}^{(1)} + e^{ik_z(z+z')} M_{22}^{(2)} + e^{ik_z(z'-z)} e^{2ik_z d} M_{22}^{(3)} + e^{-ik_z(z+z')} e^{2ik_z d} M_{22}^{(4)} \right], \quad (74)$$

$$D_{zz}^E(\omega, k_r, z, z') = \frac{ik_r^2}{2k_z} \times \left[ e^{ik_z(z-z')} e^{2ik_z d} M_{11}^{(1)} - e^{ik_z(z+z')} M_{11}^{(2)} + e^{ik_z(z'-z)} e^{2ik_z d} M_{11}^{(3)} - e^{-ik_z(z+z')} e^{2ik_z d} M_{11}^{(4)} \right]. \quad (75)$$

After integration over the polar coordinates, we express scattered electric Green’s functions for coinciding arguments  $\mathbf{r} = \mathbf{r}'$  in terms of matrix elements of matrices (56)–(59) [88]:

$$D_{xx}^E(\omega, \mathbf{r} = \mathbf{r}') = D_{yy}^E(\omega, \mathbf{r} = \mathbf{r}') = \frac{i}{8\pi} \int_0^{\infty} dk_r k_r \times \left[ k_z (e^{2ik_z d} M_{11}^{(1)} + e^{2ik_z z'} M_{11}^{(2)} + e^{2ik_z d} M_{11}^{(3)} + e^{2ik_z(d-z')} M_{11}^{(4)}) + \frac{\omega^2}{k_z} (e^{2ik_z d} M_{22}^{(1)} + e^{2ik_z z'} M_{22}^{(2)} + e^{2ik_z d} M_{22}^{(3)} + e^{2ik_z(d-z')} M_{22}^{(4)}) \right], \quad (76)$$

$$D_{zz}^E(\omega, \mathbf{r} = \mathbf{r}') = -\frac{i}{4\pi} \int_0^{\infty} dk_r \frac{k_r^3}{k_z} \times \left[ -e^{2ik_z d} M_{11}^{(1)} + e^{2ik_z z'} M_{11}^{(2)} - e^{2ik_z d} M_{11}^{(3)} + e^{2ik_z(d-z')} M_{11}^{(4)} \right]. \quad (77)$$

Scattered magnetic Green’s functions can be evaluated from reflected electric Green’s functions:

$$D_{il}^H(\omega, \mathbf{r}, \mathbf{r}') = \frac{1}{\omega^2} \epsilon_{ijk} \epsilon_{lmn} \frac{\partial}{\partial x^j} \frac{\partial}{\partial x^m} D_{kn}^E(\omega, \mathbf{r}, \mathbf{r}'). \quad (78)$$

The components of the scattered magnetic Green’s functions in a cylindrical local basis are found from (78) and (73)–(75):

$$D_{rr}^H(\omega, k_r, z, z') = \frac{ik_z}{2} \times \left[ e^{ik_z(z-z')} e^{2ik_z d} M_{22}^{(1)} + e^{ik_z(z+z')} M_{22}^{(2)} + e^{ik_z(z'-z)} e^{2ik_z d} M_{22}^{(3)} + e^{-ik_z(z+z')} e^{2ik_z d} M_{22}^{(4)} \right], \quad (79)$$

$$D_{\varphi\varphi}^H(\omega, k_r, z, z') = \frac{i\omega^2}{2k_z} \times \left[ e^{ik_z(z-z')} e^{2ik_z d} M_{11}^{(1)} - e^{ik_z(z+z')} M_{11}^{(2)} + e^{ik_z(z'-z)} e^{2ik_z d} M_{11}^{(3)} - e^{-ik_z(z+z')} e^{2ik_z d} M_{11}^{(4)} \right], \quad (80)$$

$$D_{zz}^H(\omega, k_r, z, z') = \frac{ik_r^2}{2k_z} \times \left[ e^{ik_z(z-z')} e^{2ik_z d} M_{22}^{(1)} + e^{ik_z(z+z')} M_{22}^{(2)} + e^{ik_z(z'-z)} e^{2ik_z d} M_{22}^{(3)} + e^{-ik_z(z+z')} e^{2ik_z d} M_{22}^{(4)} \right]. \quad (81)$$

The Cartesian components of the scattered magnetic Green’s functions are evaluated in complete analogy to the evaluation of the Cartesian components of the scattered electric Green’s functions.

For every  $0 < z' < d$  and the coinciding arguments of the reflected local Green’s functions  $z' = z$ , these identities hold:

$$D_{rr}^E(\omega, k_r, z', z') + D_{\varphi\varphi}^H(\omega, k_r, z', z') - D_{zz}^E(\omega, k_r, z', z') = ik_z e^{i2k_z d} \left( M_{11}^{(1)} + M_{11}^{(3)} \right), \quad (82)$$

$$D_{rr}^H(\omega, k_r, z', z') + D_{\varphi\varphi}^E(\omega, k_r, z', z') - D_{zz}^H(\omega, k_r, z', z') = ik_z e^{i2k_z d} \left( M_{22}^{(1)} + M_{22}^{(3)} \right). \quad (83)$$

The Casimir pressure  $P$  equals the  $T_{zz}$  component of the fluctuation stress tensor in a slit between half-spaces; it is expressed in terms of the scattered electric and magnetic Green’s functions:

$$P = -\frac{i}{2} \int_{-\infty}^{+\infty} \frac{d\omega}{2\pi} \left[ D_{xx}^E(\omega, \mathbf{r}, \mathbf{r}) + D_{yy}^E(\omega, \mathbf{r}, \mathbf{r}) - D_{zz}^E(\omega, \mathbf{r}, \mathbf{r}) + D_{xx}^H(\omega, \mathbf{r}, \mathbf{r}) + D_{yy}^H(\omega, \mathbf{r}, \mathbf{r}) - D_{zz}^H(\omega, \mathbf{r}, \mathbf{r}) \right]. \quad (84)$$

We use Formulas (70)–(72), identities (82)–(83) and the Wick rotation to express the Casimir pressure in terms of the reflection matrices  $R_1(i\omega)$  and  $R_2(i\omega)$ :

$$P = \frac{1}{(2\pi)^2} \int_0^\infty d\omega \int_0^\infty dk_r k_r \times \left[ D_{rr}^E(i\omega, k_r, z', z') + D_{\varphi\varphi}^E(i\omega, k_r, z', z') - D_{zz}^E(i\omega, k_r, z', z') + D_{rr}^H(i\omega, k_r, z', z') + D_{\varphi\varphi}^H(i\omega, k_r, z', z') - D_{zz}^H(i\omega, k_r, z', z') \right] = -\frac{1}{(2\pi)^2} \int_0^\infty d\omega \int_0^\infty dk_r k_r \tilde{k}_z \text{Tr} \left[ \left( I - R_2(i\omega) R_1(i\omega) e^{-2\tilde{k}_z d} \right)^{-1} R_2(i\omega) R_1(i\omega) e^{-2\tilde{k}_z d} + \left( I - R_1(i\omega) R_2(i\omega) e^{-2\tilde{k}_z d} \right)^{-1} R_1(i\omega) R_2(i\omega) e^{-2\tilde{k}_z d} \right], \quad (85)$$

where “Tr” defines the trace operation and  $\tilde{k}_z \equiv \sqrt{\omega^2 + k_r^2}$ .

The corresponding Casimir energy on a unit surface has the form

$$\frac{E}{S} = \frac{1}{(2\pi)^2} \int_0^\infty d\omega \int_0^\infty dk_r k_r \text{Tr} \ln \left( I - R_1(i\omega) R_2(i\omega) e^{-2\tilde{k}_z d} \right). \quad (86)$$

The equivalence of the Casimir energy (86) to the result for the Casimir energy obtained within the scattering approach [43] is proved in Appendix A.

### 3. Casimir Interaction in Systems with Chern–Simons Layers on Realistic Substrates

The scattering approach yields finite expressions for the Casimir energy of several interacting objects; it has been applied to diffraction gratings [93–96], spheres, cylinders and other geometries [97–107]. Planes with conductivity have also been studied in the framework of the scattering approach in Refs. [3,108–112]. The experiment [113] has confirmed the (2 + 1) finite temperature polarization operator approach in the description of graphene layers and the strong temperature dependence of the Casimir pressure for interacting layers of graphene [108].

The Casimir energy of two Chern–Simons layers in vacuum for arbitrary Chern–Simons constants  $a_1$  and  $a_2$  was derived in Ref. [42] in the framework of the scattering approach. For  $a_1 = a_2$ , the Casimir force is repulsive over an interval  $a_1 \in [0, a_{\max}]$ , where  $a_{\max} \approx 1.032502$  [41,43]. For  $a_1 = -a_2$ , the Casimir force is always attractive for two Chern–Simons layers in vacuum [42].

Suppose there is a quantization of Chern–Simons parameters  $a_1$  and  $a_2$  as in quantum Hall systems:  $a_1 = \alpha m$ ,  $a_2 = \alpha n$ , where  $m$  and  $n$  are integer numbers and  $\alpha$  is a fine structure constant. The Casimir repulsion for two half-spaces covered by Chern–Simons layers was studied for Au, intrinsic Si and SiO<sub>2</sub> glass substrate materials in Refs. [43,44]. In Ref. [43], it was shown that for two Au substrate half-spaces separated by a vacuum slit, the Casimir repulsion can be achieved at the maximum distance  $d = 3.65$  nm for  $a_1 = a_2 = 0.565$ , and for two Si substrate half-spaces, the Casimir repulsion can be achieved at the maximum distance  $d = 6.39$  nm for  $a_1 = a_2 = 0.567$ . It was demonstrated in Ref. [44] that for two SiO<sub>2</sub> substrate half-spaces separated by a vacuum slit, the Casimir repulsion can be realized at the maximum distance  $d = 26.52$  nm between half-spaces; the maximum distance at which the Casimir repulsion occurs in this system corresponds to Chern–Simons constants  $a_1 = a_2 = 0.542$  or  $m = n = 74$ . In Ref. [44], it was shown that the minimum of the Casimir energy with  $d > 10$  nm is achieved for integer  $m = n \in [34, 115]$ . The Casimir interaction of Chern–Simons layers in the presence of realistic substrate materials was not studied for small enough and different values of  $a_1$  and  $a_2$  or for geometries different from two half-space substrates with boundary Chern–Simons layers.

In this Section, we study the Casimir interaction of Chern–Simons layers for small enough values of  $a_1$  and  $a_2$  and explore the transition between the regimes of Casimir attraction and repulsion in the presence of a realistic dielectric substrate. Consider the Chern–Simons plane layer defined by the constant  $a_1$  separated by a vacuum slit of width  $d$  from a dielectric half-space characterized by a dielectric permittivity  $\varepsilon_2(\omega)$  and the boundary Chern–Simons layer defined by the constant  $a_2$  (Figure 2). We emphasize that  $\varepsilon_1(\omega) = 1$  in this case. We evaluate the Casimir energy in this system for two dielectric substrate materials: intrinsic Si and SiO<sub>2</sub> glass. For the dielectric permittivity of intrinsic Si, the model from Ref. [114] is used. For SiO<sub>2</sub> glass, we use data from [115] to evaluate dielectric permittivity at imaginary frequencies. We apply Equation (86) to evaluate the Casimir energy.

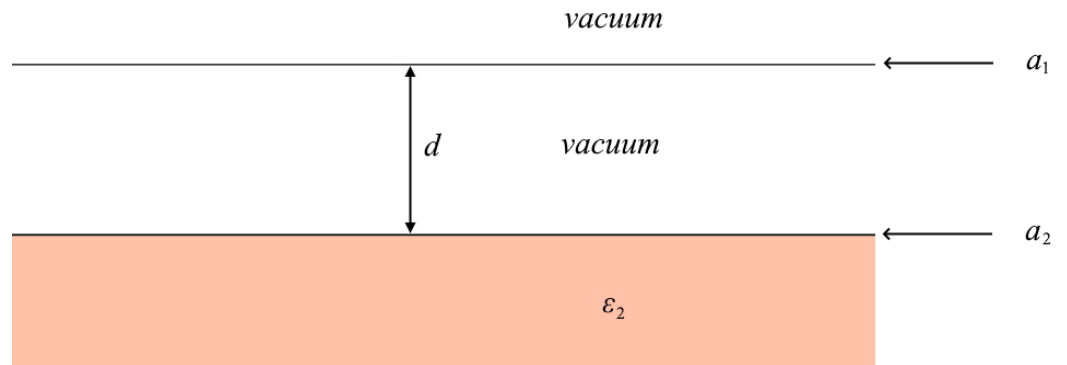


**Figure 2.** The Chern–Simons layer defined by  $a_1$  is separated by a distance  $d$  from a dielectric half-space, with the boundary Chern–Simons layer defined by  $a_2$ . The permittivity of a dielectric half-space is  $\epsilon_2$ .

The Casimir energy for the Si substrate and Chern–Simons layers with  $m = n = 1$  is presented in Figure 3; the minimum of the energy is at the distance  $d = 35.5$  nm. For  $n = 1, m = 2$ , the minimum is at the distance  $d = 17.6$  nm; for  $n = 1, m = 3$ , the minimum is at the distance  $d = 11.9$  nm.

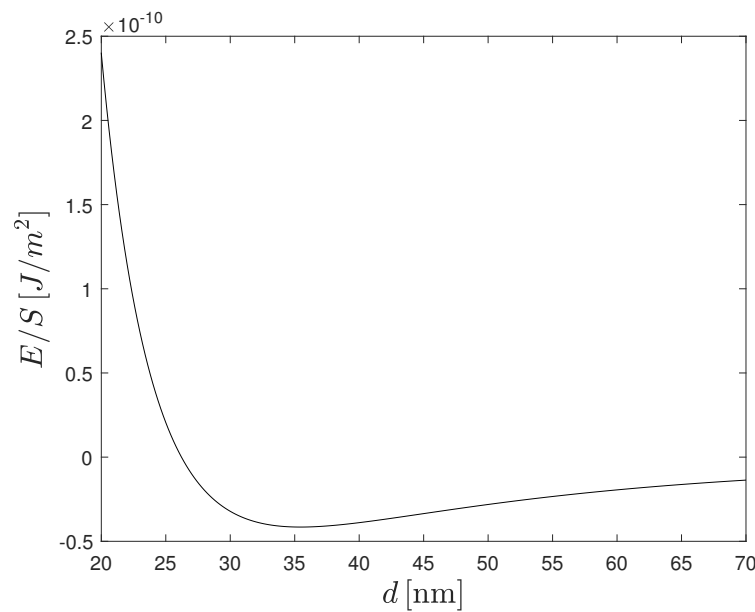


**Figure 3.** The Casimir energy (86) as a function of a distance  $d$  between the Chern–Simons layer defined by  $a_1 = \alpha$  and the Chern–Simons layer defined by  $a_2 = \alpha$  at the boundary of intrinsic Si half-space substrate.

The Casimir energy for the SiO<sub>2</sub> glass substrate and Chern–Simons plane layers with  $n = 1, m = 6$  is shown in Figure 4; the minimum of the energy is at the distance  $d = 13.7$  nm. For  $n = 1, m = 5$ , the minimum is at the distance  $d = 20$  nm; for  $n = 1, m = 4$ , the minimum is at the distance  $d = 38.2$  nm; for  $n = 1, m = 3$ , the minimum is at the distance  $d = 276$  nm; for  $n = 1, m = 2$ , the minimum is at the distance  $d = 1547$  nm. For  $n = 1, m = 1$ , there is no minimum of the Casimir energy: the Casimir repulsion occurs at all distances between the Chern–Simons layers.

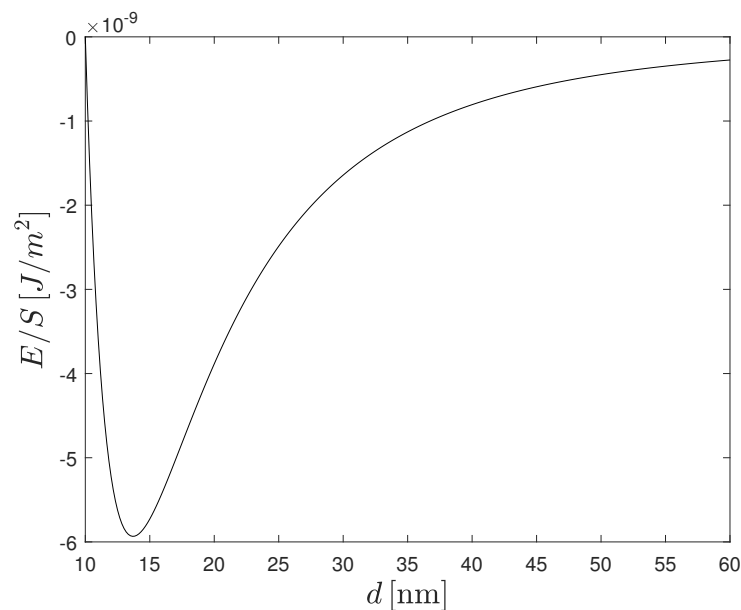


**Figure 4.** The Casimir energy (86) as a function of a distance  $d$  between the Chern–Simons layer defined by  $a_1 = 6\alpha$  and the Chern–Simons layer defined by  $a_2 = \alpha$  at the boundary of SiO<sub>2</sub> glass half-space substrate.

#### 4. Discussion and Summary

The Green’s functions scattering method [3,64] is explicitly gauge-invariant by construction; it is based on a direct evaluation of electric and magnetic Green’s functions and the fluctuation stress tensor in a vacuum slit between objects. In Refs. [3,64], the Casimir pressure is derived for flat geometries and boundary conditions when there is no mixing between transverse electric and transverse magnetic polarizations after reflection from flat boundaries. In Ref. [88] and in this paper, the method is generalized to systems with Chern–Simons plane layers; in this case, there is mixing between the transverse electric and transverse magnetic polarizations after reflection from the Chern–Simons layers.

In the present paper, the Casimir pressure is derived for dielectric half-spaces with Chern–Simons plane-parallel boundary layers via evaluation of the fluctuation stress tensor in a vacuum slit. Section 2, presents derivation of the Casimir pressure (85) expressed in terms of reflection matrices through evaluation of the fluctuation stress tensor in a vacuum slit. The fluctuation stress tensor is expressed through electric and magnetic Green’s functions in a vacuum slit. We start from evaluation of the electric Green’s functions in a vacuum slit [88]. The derivation of the magnetic Green’s functions and the stress tensor in a vacuum slit is new. To our knowledge, the Casimir pressure expressed in terms of nondiagonal reflection matrices has not been previously derived through evaluation of the vacuum stress tensor. In Appendix A, we prove the equivalence of the Casimir energy (86) to the result for the Casimir energy obtained with the scattering approach [43].

The Casimir pressure on a Chern–Simons plane layer separated by a vacuum slit from the boundary Chern–Simons layer on intrinsic Si or SiO<sub>2</sub> glass half-spaces has remarkable properties for experimental study. In Section 3, we concentrate on the case of quite small parameters  $a_1, a_2$  for the boundary Chern–Simons layers: the case that is easier to implement experimentally. The case of relatively small and different values of  $a_1, a_2$  was not investigated before. The geometry of the Chern–Simons plane layer separated by a vacuum slit from a dielectric half-space with the boundary Chern–Simons layer was not studied before. It is convenient to consider quantum Hall quantization of the parameters  $a_1 = m\alpha$ ,  $a_2 = n\alpha$ , where  $m$  and  $n$  are integer numbers. For  $m = n = 1$ , the Casimir pressure is repulsive at all separations for the SiO<sub>2</sub> substrate; however, there exists a minimum of the Casimir energy in this case for the Si substrate. For  $n = 1$  and integers  $m > 1$ , there is a

minimum of the Casimir energy both for the Si and SiO<sub>2</sub> substrates; the Casimir pressure is attractive when the separation between the layers is greater than the separation at the position of the minimum of the energy, and it is repulsive at shorter separations. We find the positions of the minimum of the Casimir energy for  $n = 1$  and  $m = 1, 2, 3$  for the intrinsic Si substrate and for  $n = 1$  and integers  $m \in [2, 6]$  for the SiO<sub>2</sub> glass substrate.

The results obtained in this paper demonstrate that intrinsic Si and SiO<sub>2</sub> glass are natural substrate materials for the study of transitions from an attractive regime of the Casimir pressure to a repulsive one. The positions of the minimum of the Casimir energy are found at experimentally realizable distances between the layers for quite small integer numbers of quantization parameters for both Chern–Simons layers, which is important for experimental realization of the repulsive Casimir force.

**Author Contributions:** Both authors contributed equally to this work. All authors have read and agreed to the published version of the manuscript.

**Funding:** This research has received financial support from a grant from the Russian Science Foundation (RSF project N<sup>o</sup> 22-13-00151).

**Data Availability Statement:** Data are contained within the article.

**Acknowledgments:** Research was performed at the Research park of the St. Petersburg State University Computing Center, Russia.

**Conflicts of Interest:** The authors declare no conflicts of interest.

### Appendix A. Representations of the Casimir Energy in Two Bases

Here, we prove the equivalence of the Casimir energy (86) to the result for the Casimir energy obtained with the scattering approach [43,44]. In the present paper, we use the local polar basis vectors  $\mathbf{e}_r$  and  $\mathbf{e}_\varphi$  in momentum space; in Ref. [43], the local basis vectors  $\mathbf{e}_s$  and  $\mathbf{e}_p$  of the TE and TM polarizations in momentum space have been used. The amplitudes of the incident electric fields in the two bases are related by the matrix  $A^f$ :

$$\begin{pmatrix} N_r \\ N_\varphi \end{pmatrix} = A^f \begin{pmatrix} N_s \\ N_p \end{pmatrix}. \tag{A1}$$

The amplitudes of the reflected electric field  $v_i$  are expressed through the amplitudes of the incident field  $N_i$  by the matrix  $R$  defined in Equation (53):

$$\begin{pmatrix} v_r \\ v_\varphi \end{pmatrix} = R \begin{pmatrix} N_r \\ N_\varphi \end{pmatrix}. \tag{A2}$$

The amplitudes of the reflected electric field in the two bases are related by the transition matrix  $A^g$ :

$$\begin{pmatrix} v_s \\ v_p \end{pmatrix} = A^g \begin{pmatrix} v_r \\ v_\varphi \end{pmatrix} = A^g R A^f \begin{pmatrix} N_s \\ N_p \end{pmatrix} = R' \begin{pmatrix} N_s \\ N_p \end{pmatrix}. \tag{A3}$$

One immediately finds the relation between the reflection matrices in the two bases:

$$R' = A^g R A^f. \tag{A4}$$

The transformation matrices for a reflection from the upper half-space have the form

$$A^{g1} = \begin{pmatrix} 0 & -1 \\ \omega/k_z & 0 \end{pmatrix}, \tag{A5}$$

$$A^{f1} = \begin{pmatrix} 0 & -k_z/\omega \\ -1 & 0 \end{pmatrix}. \tag{A6}$$

For a reflection from the lower half-space, the transformation matrices have the form

$$A^{g2} = \begin{pmatrix} 0 & -1 \\ -\omega/k_z & 0 \end{pmatrix}, \quad (\text{A7})$$

$$A^{f2} = \begin{pmatrix} 0 & k_z/\omega \\ -1 & 0 \end{pmatrix}. \quad (\text{A8})$$

From (53), (54), (A4) and (A5)–(A8), we obtain reflection matrices in agreement with the scattering approach [43]:

$$R'_1 = \frac{1}{1 + a_1^2 T_1} \begin{pmatrix} r_{\text{TE}_1} - a_1^2 T_1 & -a_1 T_1 \\ -a_1 T_1 & r_{\text{TM}_1} + a_1^2 T_1 \end{pmatrix}, \quad (\text{A9})$$

$$R'_2 = \frac{1}{1 + a_2^2 T_2} \begin{pmatrix} r_{\text{TE}_2} - a_2^2 T_2 & a_2 T_2 \\ a_2 T_2 & r_{\text{TM}_2} + a_2^2 T_2 \end{pmatrix}. \quad (\text{A10})$$

One can write the product of the reflection matrices from the upper and the lower half-spaces:

$$\begin{aligned} R'_1 R'_2 &= \begin{pmatrix} 0 & -1 \\ \omega/k_z & 0 \end{pmatrix} R_1 \begin{pmatrix} 0 & -k_z/\omega \\ -1 & 0 \end{pmatrix} \begin{pmatrix} 0 & -1 \\ -\omega/k_z & 0 \end{pmatrix} R_2 \begin{pmatrix} 0 & k_z/\omega \\ -1 & 0 \end{pmatrix} \\ &= \begin{pmatrix} 0 & -1 \\ \omega/k_z & 0 \end{pmatrix} R_1 R_2 \begin{pmatrix} 0 & k_z/\omega \\ -1 & 0 \end{pmatrix}. \end{aligned} \quad (\text{A11})$$

The equality of the trace operations in two different bases follows:

$$\text{Tr}(R'_1 R'_2)^L = \text{Tr}(R_1 R_2)^L, \quad (\text{A12})$$

where  $L$  is a positive integer number. The equivalence of the Casimir energy (86) to the result for the Casimir energy obtained with the scattering approach [43] follows from the equality (A12).

## References

1. Casimir, H.B.G.; Polder, D. The influence of retardation on the London–van der Waals forces. *Phys. Rev.* **1948**, *73*, 360–372. [CrossRef]
2. Casimir, H.B.G. On the attraction between two perfectly conducting plates. *Proc. Kon. Ned. Akad. Wetensch. B* **1948**, *51*, 793–795. Available online: <https://dwc.knaw.nl/DL/publications/PU00018547.pdf> (accessed on 1 February 2024).
3. Marachevsky, V.N.; Sidelnikov, A.A. Green functions scattering in the Casimir effect. *Universe* **2021**, *7*, 195. [CrossRef]
4. Lifshitz, E.M.; Pitaevskii, L.P. *Statistical Physics. Part 2: Theory of Condensed States*; Butterworth–Heinemann Ltd/Elsevier Ltd.: Oxford, UK, 1980. [CrossRef]
5. Barash, Y.S.; Ginzburg, V.L. Electromagnetic fluctuations in matter and molecular (Van-der-Waals) forces between them. *Sov. Phys. Usp.* **1975**, *18*, 305–322. [CrossRef]
6. Barash, Y.S.; Ginzburg, V.L. Some problems in the theory of van der Waals forces. *Sov. Phys. Usp.* **1984**, *27*, 467–491. [CrossRef]
7. Plunien, G.; Müller, B.; Greiner, W. The Casimir effect. *Phys. Rep.* **1986**, *134*, 87–193. [CrossRef]
8. Bordag, M.; Mohideen, U.; Mostepanenko, V.M. New developments in the Casimir effect. *Phys. Rep.* **2001**, *353*, 1–205. [CrossRef]
9. Santangelo, E.M. Evaluation of Casimir energies through spectral functions. *Theor. Math. Phys.* **2002**, *131*, 527–542. [CrossRef]
10. Milton, K.A. The Casimir effect: Recent controversies and progress. *J. Phys. A Math. Gen.* **2004**, *37*, R209–R277. [CrossRef]
11. Jaffe, R.L. Casimir effect and the quantum vacuum. *Phys. Rev. D* **2005**, *72*, 021301(R). [CrossRef]
12. Scheel, S.; Buhmann, S.Y. Macroscopic quantum electrodynamics—Concepts and applications. *Acta Phys. Slovaca* **2008**, *58*, 675–809. Available online: <http://www.physics.sk/aps/pub.php?y=2008&pub=aps-08-05> (accessed on 1 February 2024). [CrossRef]
13. Klimchitskaya, G.L.; Mohideen, U.; Mostepanenko, V.M. The Casimir force between real materials: Experiment and theory. *Rev. Mod. Phys.* **2009**, *81*, 1827–1885. [CrossRef]
14. Rodriguez, A.; Capasso, F.; Johnson, S. The Casimir effect in microstructured geometries. *Nat. Photon.* **2011**, *5*, 211–221. [CrossRef]
15. Marachevsky, V.N. The Casimir effect: Medium and geometry. *J. Phys. A Math. Theor.* **2012**, *45*, 374021. [CrossRef]
16. Woods, L.M.; Dalvit, D.A.R.; Tkatchenko, A.; Rodriguez-Lopez, P.; Rodriguez, A.W.; Podgornik, R. Materials perspective on Casimir and van der Waals interactions. *Rev. Mod. Phys.* **2016**, *88*, 045003. [CrossRef]

17. Woods, L.M.; Krüger, M.; Dodonov, V.V. Perspective on some recent and future developments in Casimir interactions. *Appl. Sci.* **2021**, *11*, 293. [[CrossRef](#)]
18. Lu, B.-S. The Casimir effect in topological matter. *Universe* **2021**, *7*, 237. [[CrossRef](#)]
19. Elizalde, E. *Ten Physical Applications of Spectral Zeta Functions*; Springer: Berlin/Heidelberg, Germany, 2012. [[CrossRef](#)]
20. Kirsten, K. *Spectral Functions in Mathematics and Physics*; Chapman & Hall/CRC Press/Taylor & Francis Group: Boca Raton, FL, USA, 2002. [[CrossRef](#)]
21. Fursaev, D.; Vassilevich, D. *Operators, Geometry and Quanta: Methods of Spectral Geometry in Quantum Field Theory*; Springer Science+Business Media B.V.: Dordrecht, The Netherlands, 2011.
22. Buhmann, S.Y. *Dispersion Forces I. Macroscopic Quantum Electrodynamics and Ground-State Casimir, Casimir–Polder and van der Waals Forces*; Springer: Berlin/Heidelberg, Germany, 2012. [[CrossRef](#)]
23. Buhmann, S.Y. *Dispersion Forces II. Many-Body Effects, Excited Atoms, Finite Temperature and Quantum Friction*; Springer: Berlin/Heidelberg, Germany, 2012. [[CrossRef](#)]
24. Bordag, M.; Klimchitskaya, G.L.; Mohideen, U.; Mostepanenko, V.M. *Advances in the Casimir Effect*; Oxford University Press: Oxford, UK, 2015. [[CrossRef](#)]
25. Lifshitz, E.M. The theory of molecular attractive forces between solids. *Zh. Eksp. Teor. Fiz.* **1955**, *29*, 94–110. (In Russian) English translation: *Sov. Phys. JETP* **1956**, *2*, 73–83. Available online: <http://jetp.ras.ru/cgi-bin/e/index/e/2/1/p73?a=list> (accessed on 1 February 2024).
26. Renne, M.J. Microscopic theory of retarded van der Waals forces between macroscopic dielectric bodies. *Physica* **1971**, *56*, 125–137. [[CrossRef](#)]
27. Dzyaloshinskii, I.E.; Lifshitz, E.M.; Pitaevskii, L.P. General theory of van der Waals' forces. *Sov. Phys. Usp.* **1961**, *4*, 153–176. [[CrossRef](#)]
28. Munday, J.N.; Capasso, F.; Parsegian, V.A. Measured long-range repulsive Casimir–Lifshitz forces. *Nature* **2009**, *457*, 170–173. [[CrossRef](#)] [[PubMed](#)]
29. Pirozhenko, I.; Lambrecht, A. Repulsive Casimir forces and the role of surface modes. *Phys. Rev. A* **2009**, *80*, 042510. [[CrossRef](#)]
30. Schmidt, F.; Callegari, A.; Daddi-Moussa-Ider, A.; Munkhbat, B.; Verre, R.; Shegai, T.; Käll, M.; Löwen, H.; Gambassi, A.; Volpe, G. Tunable critical Casimir forces counteract Casimir–Lifshitz attraction. *Nat. Phys.* **2023**, *19*, 271–278. [[CrossRef](#)]
31. Tomaš, M.S. Casimir force between dispersive magnetodielectrics. *Phys. Lett. A* **2005**, *342*, 381–388. [[CrossRef](#)]
32. Geyer, B.; Klimchitskaya, G.L.; Mostepanenko, V.M. Thermal Casimir interaction between two magnetodielectric plates. *Phys. Rev. B* **2010**, *81*, 104101. [[CrossRef](#)]
33. Inui, N. Thickness dependence of the Casimir force between a magnetodielectric plate and a diamagnetic plate. *Phys. Rev. A* **2011**, *84*, 052505. [[CrossRef](#)]
34. Brevik, I.; Parashar, P.; Shajesh, K.V. Casimir force for magnetodielectric media. *Phys. Rev. A* **2018**, *98*, 032509. [[CrossRef](#)]
35. Shelden, C.; Spreng, B.; Munday, J.N. Enhanced repulsive Casimir forces between gold and thin magnetodielectric plates. *Phys. Rev. A* **2023**, *108*, 032817. [[CrossRef](#)]
36. Boyer, T.H. Van der Waals forces and zero-point energy for dielectric and permeable materials. *Phys. Rev. A* **1974**, *9*, 2078–2084. [[CrossRef](#)]
37. Rosa, F.S.S.; Dalvit, D.A.R.; Milonni, P.W. Casimir–Lifshitz theory and metamaterials. *Phys. Rev. Lett.* **2008**, *100*, 183602. [[CrossRef](#)]
38. Rosa, F.S.S.; Dalvit, D.A.R.; Milonni, P.W. Casimir interactions for anisotropic magnetodielectric metamaterials. *Phys. Rev. A* **2008**, *78*, 032117. [[CrossRef](#)]
39. Yannopoulos, V.; Vitanov, N.V. First-principles study of Casimir repulsion in metamaterials. *Phys. Rev. Lett.* **2009**, *103*, 120401. [[CrossRef](#)] [[PubMed](#)]
40. Zhao, R.; Zhou, J.; Koschny, T.; Economou, E.N.; Soukoulis, C.M. Repulsive Casimir force in chiral metamaterials. *Phys. Rev. Lett.* **2009**, *103*, 103602. [[CrossRef](#)] [[PubMed](#)]
41. Markov, V.N.; Pis'mak, Y.M. Casimir effect for thin films in QED. *J. Phys. A Math. Gen.* **2006**, *39*, 6525–6532. [[CrossRef](#)]
42. Marachevsky, V.N. Casimir effect for Chern–Simons layers in the vacuum. *Theor. Math. Phys.* **2017**, *190*, 315–320. [[CrossRef](#)]
43. Marachevsky, V.N. Casimir interaction of two dielectric half spaces with Chern–Simons boundary layers. *Phys. Rev. B* **2019**, *99*, 075420. [[CrossRef](#)]
44. Marachevsky, V.N. Chern–Simons boundary layers in the Casimir effect. *Mod. Phys. Lett. A* **2020**, *35*, 2040015. [[CrossRef](#)]
45. Pavlovsky, O.; Ulybyshev, M. Casimir energy calculations within the formalism of noncompact lattice QED. *Int. J. Mod. Phys. A* **2010**, *25*, 2457–2473. [[CrossRef](#)]
46. Pavlovsky, O.V.; Ulybyshev, M.V. Casimir energy in noncompact lattice electrodynamics. *Theor. Math. Phys.* **2010**, *164*, 1051–1063. [[CrossRef](#)]
47. Milton, K.A.; Ng, Y.J. Maxwell–Chern–Simons Casimir effect. *Phys. Rev. D* **1990**, *42*, 2875–2880. [[CrossRef](#)]
48. Elizalde, E.; Vassilevich, D.V. Heat kernel coefficients for Chern–Simons boundary conditions in QED. *Class. Quantum Gravity* **1999**, *16*, 813–822. [[CrossRef](#)]
49. Bordag, M.; Vassilevich, D.V. Casimir force between Chern–Simons surfaces. *Phys. Lett. A* **2000**, *268*, 75–80. [[CrossRef](#)]
50. Qi, X.-L.; Li, R.; Zang, J.; Zhang, S.-C. Inducing a magnetic monopole with topological surface states. *Science* **2009**, *323*, 1184–1187. [[CrossRef](#)] [[PubMed](#)]

51. Grushin, A.G.; Cortijo, A. Tunable Casimir repulsion with three-dimensional topological insulators. *Phys. Rev. Lett.* **2011**, *106*, 020403. [[CrossRef](#)] [[PubMed](#)]
52. Grushin, A.G.; Rodriguez-Lopez, P.; Cortijo, A. Effect of finite temperature and uniaxial anisotropy on the Casimir effect with three-dimensional topological insulators. *Phys. Rev. B* **2011**, *84*, 045119. [[CrossRef](#)]
53. Chen, L.; Wan, S. Casimir interaction between topological insulators with finite surface band gap. *Phys. Rev. B* **2011**, *84*, 075149. [[CrossRef](#)]
54. Chen, L.; Wan, S. Critical surface band gap of repulsive Casimir interaction between three-dimensional topological insulators at finite temperature. *Phys. Rev. B* **2012**, *85*, 115102. [[CrossRef](#)]
55. Martín-Ruiz, A.; Cambiaso, M.; Urrutia, L.F. A Green's function approach to the Casimir effect on topological insulators with planar symmetry. *Europhys. Lett.* **2016**, *113*, 60005. [[CrossRef](#)]
56. Fialkovsky, I.; Khusnutdinov, N.; Vassilevich, D. Quest for Casimir repulsion between Chern–Simons surfaces. *Phys. Rev. B* **2018**, *97*, 165432. [[CrossRef](#)]
57. Weng, H.; Yu, R.; Hu, X.; Dai, X.; Fang, Z. Quantum anomalous Hall effect and related topological electronic states. *Adv. Phys.* **2015**, *64*, 227–282. [[CrossRef](#)]
58. Liu, C.-X.; Zhang, S.-C.; Qi, X.-L. The quantum anomalous Hall effect: Theory and experiment. *Annu. Rev. Cond. Matter. Phys.* **2016**, *7*, 301–321. [[CrossRef](#)]
59. Ren, Y.; Qiao, Z.; Niu, Q. Topological phases in two-dimensional materials: A review. *Rep. Prog. Phys.* **2016**, *79*, 066501. [[CrossRef](#)] [[PubMed](#)]
60. Rodriguez-Lopez, P.; Grushin, A.G. Repulsive Casimir effect with Chern insulators. *Phys. Rev. Lett.* **2014**, *112*, 056804. [[CrossRef](#)] [[PubMed](#)]
61. Muniz, Y.; Farina, C.; Kort-Kamp, W.J.M. Casimir forces in the flatland: Interplay between photoinduced phase transitions and quantum Hall physics. *Phys. Rev. Res.* **2021**, *3*, 023061. [[CrossRef](#)]
62. Tse, W.-K.; MacDonald, A.H. Quantized Casimir force. *Phys. Rev. Lett.* **2012**, *109*, 236806. [[CrossRef](#)] [[PubMed](#)]
63. Ezawa, Z.F. *Quantum Hall Effects: Field Theoretical Approach and Related Topics*; World Scientific: Singapore, 2008. . [[CrossRef](#)]
64. Marachevsky, V.N.; Sidelnikov, A.A. Gauge-invariant derivation of the Casimir–Lifshitz pressure. *Phys. Part. Nucl. Lett.* **2023**, *20*, 1114–1116. . [[CrossRef](#)]
65. Barton, G. Quantum-electrodynamic level shifts between parallel mirrors: Analysis. *Proc. R. Soc. Lond. A* **1987**, *410*, 141–174.
66. Brevik, I.; Lygren, M.; Marachevsky, V.N. Casimir–Polder effect for a perfectly conducting wedge. *Ann. Phys.* **1998**, *267*, 134–142. [[CrossRef](#)]
67. Messina, R.; Dalvit, D.A.R.; Maia Neto, P.A.; Lambrecht, A.; Reynaud, S. Dispersive interactions between atoms and nonplanar surfaces. *Phys. Rev. A* **2009**, *80*, 022119. [[CrossRef](#)]
68. Bender, H.; Stehle, C.; Zimmermann, C.; Slama, S.; Fiedler, J.; Scheel, S.; Buhmann, S.Y.; Marachevsky, V.N. Probing atom-surface interactions by diffraction of Bose-Einstein condensates. *Phys. Rev. X* **2014**, *4*, 011029. [[CrossRef](#)]
69. Levin, M.; McCauley, A.P.; Rodriguez, A.W.; Homer Reid, M.T.; Johnson, S.G. Casimir repulsion between metallic objects in vacuum. *Phys. Rev. Lett.* **2010**, *105*, 090403. [[CrossRef](#)] [[PubMed](#)]
70. Eberlein, C.; Zietal, R. Casimir–Polder interaction between a polarizable particle and a plate with a hole. *Phys. Rev. A* **2011**, *83*, 052514. [[CrossRef](#)]
71. Buhmann, S.Y.; Marachevsky, V.N.; Scheel, S. Impact of anisotropy on the interaction of an atom with a one-dimensional nano-grating. *Int. J. Mod. Phys. A* **2016**, *31*, 1641029. [[CrossRef](#)]
72. Milton, K.A.; Abalo, E.K.; Parashar, P.; Pourtolami, N.; Brevik, I.; Ellingsen, S.A. Casimir–Polder repulsion near edges: Wedge apex and a screen with an aperture. *Phys. Rev. A* **2011**, *83*, 062507. [[CrossRef](#)]
73. Milton, K.A.; Parashar, P.; Pourtolami, N.; Brevik, I. Casimir–Polder repulsion: Polarizable atoms, cylinders, spheres, and ellipsoids. *Phys. Rev. D* **2012**, *85*, 025008. [[CrossRef](#)]
74. Milton, K.A.; Abalo, E.K.; Parashar, P.; Pourtolami, N.; Brevik, I.; Ellingsen, S.A. Repulsive Casimir and Casimir–Polder forces. *J. Phys. A Math. Theor.* **2012**, *45*, 374006. [[CrossRef](#)]
75. Shajesh, K.V.; Schaden, M. Repulsive long-range forces between anisotropic atoms and dielectrics. *Phys. Rev. A* **2012**, *85*, 012523. [[CrossRef](#)]
76. Marchetta, J.J.; Parashar, P.; Shajesh, K.V. Geometrical dependence in Casimir–Polder repulsion. *Phys. Rev. A* **2021**, *104*, 032209. [[CrossRef](#)]
77. Savin, V.P.; Koksharov, Y.A. Electrostatic repulsion between an uncharged or slightly charged conductor and a point charge. *J. Electrostat.* **2022**, *120*, 103769. [[CrossRef](#)]
78. Nogueira, E.C.M.; Queiroz, L.; Alves, D.T. Sign inversion in the lateral van der Waals force. *Phys. Rev. A* **2022**, *105*, 062816. [[CrossRef](#)]
79. Queiroz, L.; Nogueira, E.C.M.; Alves, D.T. Sign inversion in the lateral van der Waals force between an anisotropic particle and a plane with a hemispherical protuberance: An exact calculation. *J. Phys. A Math. Theor.* **2023**, *56*, 115301. [[CrossRef](#)]
80. Alves, D.T.; Queiroz, L.; Nogueira, E.C.M.; Peres, N.M.R. Curvature-induced repulsive effect on the lateral Casimir–Polder–van der Waals force. *Phys. Rev. A* **2023**, *107*, 062821. [[CrossRef](#)]
81. Venkataram, P.S.; Molesky, S.; Chao, P.; Rodriguez, A.W. Fundamental limits to attractive and repulsive Casimir–Polder forces. *Phys. Rev. A* **2020**, *101*, 052115. [[CrossRef](#)]

82. Marachevsky, V.N.; Pis'mak, Y.M. Casimir–Polder effect for a plane with Chern–Simons interaction. *Phys. Rev. D* **2010**, *81*, 065005. [[CrossRef](#)]
83. Jiang, Q.-D.; Wilczek, F. Chiral Casimir forces: Repulsive, enhanced, tunable. *Phys. Rev. B* **2019**, *99*, 125403. [[CrossRef](#)]
84. Høye, J.S.; Brevik, I. Casimir force between ideal metal plates in a chiral vacuum. *Eur. Phys. J. Plus* **2020**, *135*, 271. [[CrossRef](#)]
85. Butcher, D.T.; Buhmann, S.Y.; Scheel, S. Casimir–Polder forces between chiral objects. *New J. Phys.* **2012**, *14*, 113013. [[CrossRef](#)]
86. Khriplovich, I.B. *Parity Nonconservation in Atomic Phenomena*; Gordon and Breach Science Publishers S.A: Philadelphia, PA, USA, 1991.
87. Buhmann, S.Y.; Marachevsky, V.N.; Scheel, S. Charge-parity-violating effects in Casimir–Polder potentials. *Phys. Rev. A* **2018**, *98*, 022510. [[CrossRef](#)]
88. Marachevsky, V.N.; Sidelnikov, A.A. Casimir–Polder interaction with Chern–Simons boundary layers. *Phys. Rev. D* **2023**, *107*, 105019. [[CrossRef](#)]
89. Brown, L.S.; Maclay, G.J. Vacuum stress between conducting plates: An image solution. *Phys. Rev.* **1969**, *184*, 1272–1279. [[CrossRef](#)]
90. Weyl, H. Ausbreitung elektromagnetischer Wellen über einen Leiter. *Ann. Der Phys.* **1919**, *365*, 481–500. [[CrossRef](#)]
91. Obukhov, Y.N.; Hehl, F.W. Measuring a piecewise constant axion field in classical electrodynamics. *Phys. Lett. A* **2005**, *341*, 357–365. [[CrossRef](#)]
92. Pis'mak, D.Y.; Pis'mak, Y.M.; Wegner, F.J. Electromagnetic waves in a model with Chern–Simons potential. *Phys. Rev. E* **2015**, *92*, 013204. [[CrossRef](#)] [[PubMed](#)]
93. Lambrecht, A.; Marachevsky, V.N. Casimir interaction of dielectric gratings. *Phys. Rev. Lett.* **2008**, *101*, 160403. [[CrossRef](#)] [[PubMed](#)]
94. Lambrecht, A.; Marachevsky, V.N. Theory of the Casimir effect in one-dimensional periodic dielectric systems. *Int. J. Mod. Phys. A* **2009**, *24*, 1789–1795. [[CrossRef](#)]
95. Antezza, M.; Chan, H.B.; Guizal, B.; Marachevsky, V.N.; Messina, R.; Wang, M. Giant Casimir torque between rotated gratings and the  $\theta = 0$  anomaly. *Phys. Rev. Lett.* **2020**, *124*, 013903. [[CrossRef](#)]
96. Marachevsky, V.N. The Casimir effect for diffraction gratings, symmetry breaking and geometric transitions. *Phys. Part. Nucl. Lett.* **2023**, *20*, 255–258. [[CrossRef](#)]
97. Emig, T.; Graham, N.; Jaffe, R.L.; Kardar, M. Casimir forces between arbitrary compact objects. *Phys. Rev. Lett.* **2007**, *99*, 170403. [[CrossRef](#)]
98. Rahi, S.J.; Emig, T.; Graham, N.; Jaffe, R.L.; Kardar, M. Scattering theory approach to electromagnetic Casimir forces. *Phys. Rev. D* **2009**, *80*, 085021. [[CrossRef](#)]
99. Emig, T.; Jaffe, R.L.; Kardar, M.; Scardicchio, A. Casimir interaction between a plate and a cylinder. *Phys. Rev. Lett.* **2006**, *96*, 080403. [[CrossRef](#)]
100. Canaguier-Durand, A.; Maia Neto, P.A.; Cavero-Pelaez, I.; Lambrecht, A.; Reynaud, S. Casimir interaction between plane and spherical metallic surfaces. *Phys. Rev. Lett.* **2009**, *102*, 230404. [[CrossRef](#)] [[PubMed](#)]
101. Canaguier-Durand, A.; Gérardin, A.; Guérout, R.; Maia Neto, P.A.; Nesvizhevsky, V.V.; Voronin, A.Y.; Lambrecht, A.; Reynaud, S. Casimir interaction between a dielectric nanosphere and a metallic plane. *Phys. Rev. A* **2011**, *83*, 032508. [[CrossRef](#)]
102. Bordag, M.; Nikolaev, V. Casimir force for a sphere in front of a plane beyond proximity force approximation. *J. Phys. A Math. Theor.* **2008**, *41*, 164002. [[CrossRef](#)]
103. Bordag, M.; Pirozhenko, I. Vacuum energy between a sphere and a plane at finite temperature. *Phys. Rev. D* **2010**, *81*, 085023. [[CrossRef](#)]
104. Bordag, M.; Pirozhenko, I.G. On the Casimir entropy for a ball in front of a plane. *Phys. Rev. D* **2010**, *82*, 125016. [[CrossRef](#)]
105. Rodriguez-Lopez, P.; Rahi, S.J.; Emig, T. Three-body Casimir effects and nonmonotonic forces. *Phys. Rev. A* **2009**, *80*, 022519. [[CrossRef](#)]
106. Graham, N.; Shpunt, A.; Emig, T.; Rahi, S.J.; Jaffe, R.L.; Kardar, M. Electromagnetic Casimir forces of parabolic cylinder and knife-edge geometries. *Phys. Rev. D* **2011**, *83*, 125007. [[CrossRef](#)]
107. Rodriguez-Lopez, P.; Emig, T.; Noruzifar, E.; Zandi, R. Effect of curvature and confinement on the Casimir–Polder interaction. *Phys. Rev. A* **2015**, *91*, 012516. [[CrossRef](#)]
108. Fialkovsky, I.V.; Marachevsky, V.N.; Vassilevich, D.V. Finite-temperature Casimir effect for graphene. *Phys. Rev. B* **2011**, *84*, 035446. [[CrossRef](#)]
109. Klimchitskaya, G.L.; Mostepanenko, V.M. Casimir and Casimir–Polder forces in graphene systems: Quantum field theoretical description and thermodynamics. *Universe* **2020**, *6*, 150. [[CrossRef](#)]
110. Khusnutdinov, N.; Kashapov, R.; Woods, L.M. Casimir–Polder effect for a stack of conductive planes. *Phys. Rev. A* **2016**, *94*, 012513. [[CrossRef](#)]
111. Khusnutdinov, N.; Kashapov, R.; Woods, L.M. Thermal Casimir and Casimir–Polder interactions in N parallel 2D Dirac materials. *2D Mater.* **2018**, *5*, 035032. [[CrossRef](#)]
112. Antezza, M.; Fialkovsky, I.; Khusnutdinov, N. Casimir–Polder force and torque for anisotropic molecules close to conducting planes and their effect on CO<sub>2</sub>. *Phys. Rev. B* **2020**, *102*, 195422. [[CrossRef](#)]
113. Liu, M.; Zhang, Y.; Klimchitskaya, G.L.; Mostepanenko, V.M.; Mohideen, U. Demonstration of an unusual thermal effect in the Casimir force from graphene. *Phys. Rev. Lett.* **2021**, *126*, 206802. [[CrossRef](#)]

- 
114. Lambrecht, A.; Pirozhenko, I.; Duraffourg, L.; Andreucci, P. The Casimir effect for silicon and gold slabs. *Europhys. Lett.* **2007**, *77*, 44006. [[CrossRef](#)]
  115. Palik, E.D. (Ed.) *Handbook of Optical Constants of Solids*; Academic Press/Elsevier Inc.: Cambridge, MA, USA, 1997. Available online: <https://www.sciencedirect.com/book/9780125444156/handbook-of-optical-constants-of-solids> (accessed on 1 February 2024).

**Disclaimer/Publisher's Note:** The statements, opinions and data contained in all publications are solely those of the individual author(s) and contributor(s) and not of MDPI and/or the editor(s). MDPI and/or the editor(s) disclaim responsibility for any injury to people or property resulting from any ideas, methods, instructions or products referred to in the content.